

Dynamics of Excited Electrons in Copper and Ferromagnetic Transition Metals: Theory and Experiment

R. Knorren* and K.H. Bennemann

Institut für Theoretische Physik, Freie Universität Berlin, Arnimallee 14, D-14195 Berlin, Germany

R. Burgermeister

Laboratorium für Festkörperphysik, ETH Zürich, 8093 Zürich, Switzerland

M. Aeschlimann†

Laboratorium für Technische Chemie, ETH Zürich, 8092 Zürich, Switzerland

(September 21, 2018)

Both theoretical and experimental results for the dynamics of photoexcited electrons at surfaces of Cu and the ferromagnetic transition metals Fe, Co, and Ni are presented. A model for the dynamics of excited electrons is developed, which is based on the Boltzmann equation and includes effects of photoexcitation, electron-electron scattering, secondary electrons (cascade and Auger electrons), and transport of excited carriers out of the detection region. From this we determine the time-resolved two-photon photoemission (TR-2PPE). Thus a direct comparison of calculated relaxation times with experimental results by means of TR-2PPE becomes possible. The comparison indicates that the magnitudes of the spin-averaged relaxation time τ and of the ratio $\tau_{\uparrow}/\tau_{\downarrow}$ of majority and minority relaxation times for the different ferromagnetic transition metals result not only from density-of-states effects, but also from different Coulomb matrix elements M . Taking $M_{\text{Fe}} > M_{\text{Cu}} > M_{\text{Ni}} = M_{\text{Co}}$ we get reasonable agreement with experiments.

I. INTRODUCTION

The dynamics of excited electrons at metal surfaces has been studied intensively over the last few years. It is of high interest to understand the dynamics of non-equilibrium electrons in different metals on a femtosecond timescale and its influence on chemical reactions at surfaces, for example. From the relaxation of hot electrons in ferromagnets one may also learn about the decay of transient magnetization and about spin-selective transport and tunneling.

Short laser pulses of 15–50 fs duration and the pump-probe technique have made possible the study of electronic dynamics on ultrashort timescales comparable to typical electron-electron interaction timescales, which in metals are of the order of 5–50 fs for excitation energies of about 1–2 eV.

The aim of 2PPE experiments is to study the relaxation of single excited electrons. A relaxation time is extracted from the width of the 2PPE signal as a function of the delay time between pump and probe pulses.¹ In the earlier experiments,^{1,2} the relaxation time was interpreted as the lifetime of a single excited electron due to the Coulomb interaction. It was compared to the theoretical result from Fermi-liquid theory (FLT).³ The order of magnitude and the energy dependence of the FLT lifetime were in good agreement with the experimental results.^{1,2,4,5} However, it was realized that additional physical effects such as the transport of excited electrons out of the detection region and the secondary-electron cascade come into play.^{1,4,6} It was noted that in 2PPE one generally observes the relaxation of a nascent photoexcited electron population and not only the lifetime of a single excited electron. For low excitation energies, electronic lifetimes are longer than a few tens of fs, and ballistic transport leads to a removal of electrons from the probed region.⁷ This is indistinguishable from a stronger electronic decay. Furthermore, under certain conditions the measured relaxation time shows a surprising non-monotonous feature which depends on the photon energy of the exciting laser, which cannot be explained by a single-electron lifetime and transport.^{8–10} It was pointed out that the holes left behind in the excitation can influence the observed relaxation time of hot electrons.^{10,11} One explanation was that secondary electrons generated by the filling of holes (Auger electrons) are responsible for the non-monotonous behavior.¹⁰ However, the contribution of Auger electrons to the relaxation time has raised some controversy. Petek *et al.* have argued that Auger electrons do not make a significant contribution to the observed 2PPE signal and to the relaxation time at high intermediate-state energies $E - E_F > 1.5 - 2$ eV.^{12,13}

The 3d transition metals have not been as intensely studied as the noble metals. However, they offer several interesting features which make it worth to study them in detail. They offer the opportunity to study spin-dependent interactions if the spin of the emitted electrons is measured.^{14,15} Furthermore, the closeness of the *d* bands to the

Fermi energy makes it possible to study electronic interactions not only for free-electron-like states, but also for the more localized d -electron states.

On the theoretical side, the effect of the density of states (DOS) on the lifetime and the influence of secondary electrons in photoemission from transition metals have been addressed by Penn *et al.*¹⁶ Using a similar approach, Zarate *et al.*¹⁷ have calculated low-energy-electron lifetimes in noble metals and ferromagnetic Co. First-principles lifetime calculations have been performed for image-potential states¹⁸ and for bulk states in alkali and noble metals.^{19,20} The lifetime is obtained from the inverse of the imaginary part of the self-energy. As in FLT, the lifetime calculated in the above works is a single-electron lifetime. Due to the additional effects of secondary electrons and transport in 2PPE experiments, it is difficult to compare these theoretical results with the relaxation times measured in 2PPE. For the $3d$ transition metals Fe, Co, and Ni, which show important contributions from the more localized d states in the vicinity of the Fermi energy, first-principles lifetime calculations in the range of a few eV above the Fermi energy have not, to our knowledge, been reported in the literature so far.

In this paper, we present both theoretical and experimental results for the electron dynamics as observed in 2PPE for Cu and ferromagnetic Fe, Co, and Ni. Systematic trends among the transition metals are discussed. A theoretical model for the 2PPE process is presented which is based on the time evolution of the distribution function. The latter is calculated with the Boltzmann equation including effects of photoexcitation, electron-electron scattering and transport. Electron-electron scattering rates are calculated from a golden-rule expression using realistic DOS and constant Coulomb matrix elements. The approach for the calculation of the scattering rates is as outlined by Penn *et al.*¹⁶ We extend this approach to include not only the relaxation of excited electrons, but also the generation of secondary electrons. Rather than performing a first-principles calculation of the lifetime of single excited electrons, we lay emphasis on using a model which yields material-specific single-electron lifetimes for transition metals and enables us to calculate the relaxation time of the distribution including effects of secondary electrons and transport. This allows a direct comparison of calculated relaxation times with experimental results.

The structure of the paper is as follows. In Sec. II, we describe the model for the dynamics of excited electrons from which 2PPE is calculated. Numerical results for the relaxation of the distribution of excited electrons are presented in Sec. III. In Sec. IV, the experiments are described and their results are given. In Sec. V, experimental and theoretical results are compared and discussed. Conclusions and outlook are given in Sec. VI.

II. THEORY

The process of two-photon photoemission is illustrated in Fig. 1. The intensity $I^{2\text{PPE}}$ is obtained by multiplying the distribution function in the intermediate state $f(E, \sigma, z, t)$ with a factor e^{-z/λ_σ} for transmission into the vacuum²¹ and with the power of the laser pulse $P(t)$ and integrating over time t and coordinate z perpendicular to the surface:

$$I^{2\text{PPE}}(E + h\nu, \sigma) = \int_{-\infty}^{\infty} dt P(t) \int_0^{\infty} dz e^{-z/\lambda_\sigma} f(E, \sigma, z, t). \quad (1)$$

Energy and spin of the intermediate state are denoted by E and σ . The photon frequency is given by ν . For the transmission factor, we use the spin-averaged values of the attenuation length λ measured in overlayer experiments for different elements.²² The above expression for the photoemission intensity based on the distribution function is suited for the description of the population dynamics. Our aim here is to describe incoherent electronic processes like the decay of excited electrons and the generation of secondary electrons due to electron-electron scattering. Also, the experiments with which we wish to compare our calculations are phase-averaged measurements of the decay of the population of excited electrons. The expression is further justified by the fact that for bulk states in metals, one expects rapid loss of coherence within a few fs. However, clearly, if one is mainly interested in coherent effects like the decay of the optically induced polarization, the treatment of the dynamics and the photoemission process should be based on both occupation function and polarization.^{2,23,24} Recent interferometric measurements have shown relatively long decoherence times in Cu of $T_2^\omega = 5 - 10$ fs for holes at the top of the d bands and electrons at about $E - E_F = 1$ eV and up to $T_2^{2\omega} = 35$ fs for electrons at about $E - E_F = 4$ eV.²⁵

As shown in Fig. 1, 2PPE involves three electronic states, in which electron-electron scattering, electronic transport and emission into the vacuum take place and determine the observed photoemission signal. After optical excitation, the holes left behind in the initial state relax and get filled via Coulomb scattering by electrons from occupied levels closer to the Fermi energy. Energy conservation requires that at the same time other electrons from below the Fermi energy are excited to unoccupied levels above the Fermi energy (secondary electrons). The holes are also filled via transport processes by electrons from the bulk. The optically excited (primary) electrons are scattered out of the intermediate state by scattering with electrons in the Fermi sea. On the other hand, secondary electrons are scattered into the intermediate state, which leads to the refilling of this state. The intermediate state can be refilled by: i) an

optically excited (hot) electron after an electron-electron scattering process; ii) a cold electron from below the Fermi energy after scattering with a hot electron; iii) an Auger electron (an electron excited from below the Fermi energy after a hole is filled by a cold electron). The latter process leads to a dependence of the observed lifetime on the rate of filling of holes (the inverse hole lifetime). The transport of excited electrons into the bulk leads to the removal of electrons from the intermediate state. Thirdly, the final state is above the vacuum energy and describes a free electron which can escape from the solid. Only electrons within a mean free path of the surface absorbing a second photon are emitted into the vacuum.

We use now the Boltzmann equation taking into account the above processes to describe the time evolution of the electronic distribution function. The electronic states are characterized by energy E , spin σ , band index $\alpha = sp, d$ and coordinate z perpendicular to the surface. The Boltzmann equation reads

$$\frac{\partial f(E\alpha\sigma z)}{\partial t} = \frac{\partial f(E\alpha\sigma z)}{\partial t} \Big|_{\text{optical}} + \frac{\partial f(E\alpha\sigma z)}{\partial t} \Big|_{e-e}^{\text{in}} + \frac{\partial f(E\alpha\sigma z)}{\partial t} \Big|_{e-e}^{\text{out}} + \frac{\partial f(E\alpha\sigma z)}{\partial t} \Big|_{\text{trans}} \quad (2)$$

and contains the rates of change of the occupation due to optical excitation, electron-electron scattering and electronic transport. Note, the relaxation time τ of the intermediate state which is compared with the experimental one is determined from the decay of the occupation. The details of the procedure are described in App. A.

For the ferromagnetic metals, we calculate the relaxation time for excited spin-up and spin-down electrons, τ_{\uparrow} and τ_{\downarrow} . Spin-up and spin-down electrons will be denoted as majority and minority electrons in the following. The spin-averaged relaxation time τ is defined as $1/\tau = 1/2 (1/\tau_{\uparrow} + 1/\tau_{\downarrow})$ and the relaxation time ratio as $R = \tau_{\uparrow}/\tau_{\downarrow}$.

The optical transition rate between two electronic states due to the interaction with the laser field with photon energy $h\nu$ is given by

$$\frac{\partial f(E\alpha\sigma)}{\partial t} \Big|_{\text{optical}} = - \sum_{E',\beta} |p(E\alpha, E'\beta, \nu)|^2 f(E\alpha\sigma) [1 - f(E'\beta\sigma)] \rho(E'\beta\sigma) \delta(E - E' + h\nu). \quad (3)$$

Here, $p(E\alpha, E'\beta, \nu)$ is an average over electron momenta of the optical transition matrix elements describing the transition between an initial occupied state in band α at energy E and a final unoccupied state in band β at energy E' . The DOS in the final state is denoted by $\rho(E'\beta\sigma)$. We use energy-independent optical transition matrix elements. Thus, the strength of the optical excitation is proportional to the initial and final DOS. Optical excitation takes place within the optical penetration depth of the surface and has the time dependence of the laser field. We assume weak optical excitations, since the energy deposited in the system is not enough to significantly disturb the temperature or magnetization. The fraction of excited electrons per atom is about 10^{-6} (see Sec. IV).

The transition rates due to electron-electron scattering are calculated using Fermi's golden rule in the random- \mathbf{k} approximation, since the strong electron-electron interaction in noble and transition metals leads to a fast redistribution of electronic momenta so that the information about the initial optical excitation process in \mathbf{k} space is quickly lost. This then justifies the random- \mathbf{k} approximation for the calculation of electronic dynamics. We extend the treatment by Penn *et al.*¹⁶ to a non-equilibrium situation by calculating scattering rates into and out of a level and taking into account the non-equilibrium distribution of electrons. The scattering rates are derived in App. B. The expressions for the transition rates for scattering out of or into a state with energy E and spin $\sigma = \uparrow, \downarrow$ are given by:

$$\frac{\partial f_{E\sigma}}{\partial t} \Big|_{e-e}^{\text{out}} = -f_{E\sigma} \frac{1}{2} \int_{-\infty}^{\infty} dE' \left\{ h_{E'\sigma} W(E\sigma, E'\sigma) + h_{E'\bar{\sigma}} W(E\sigma, E'\bar{\sigma}) \right\} \quad (4)$$

and

$$\frac{\partial f_{E\sigma}}{\partial t} \Big|_{e-e}^{\text{in}} = (1 - f_{E\sigma}) \frac{1}{2} \int_{-\infty}^{\infty} dE' \left\{ e_{E'\sigma} W(E'\sigma, E\sigma) + e_{E'\bar{\sigma}} W(E'\bar{\sigma}, E\sigma) \right\}, \quad (5)$$

with

$$W(E\sigma, E'\sigma) = \frac{2\pi}{\hbar} \int_{-\infty}^{\infty} d\varepsilon \left(e_{\varepsilon\sigma} h_{\varepsilon+\omega, \sigma} 2 |M^{\uparrow\uparrow}|^2 + e_{\varepsilon\bar{\sigma}} h_{\varepsilon+\omega, \bar{\sigma}} |M^{\uparrow\downarrow}|^2 \right) \quad (6)$$

and

$$W(E\sigma, E'\bar{\sigma}) = \frac{2\pi}{\hbar} \int_{-\infty}^{\infty} d\varepsilon e_{\varepsilon\bar{\sigma}} h_{\varepsilon+\omega, \sigma} |M^{\uparrow\downarrow}|^2. \quad (7)$$

Here, $e_{E\sigma} = \rho_{E\sigma} f_{E\sigma}$ is the number of electrons and $h_{E\sigma} = \rho_{E\sigma}(1 - f_{E\sigma})$ is the number of holes at energy E , with spin σ . The energies involved in the transition are E, E', ε and $\varepsilon + \omega$, where $\omega = E - E'$ is the energy transferred in the transition. The spin is denoted by σ and its opposite by $\bar{\sigma}$. For details see App. B.

To include transport effects, we use a spatially dependent distribution function. Due to the fact that the laser spot is much larger than the optical penetration depth, we neglect transport in the direction parallel to the surface and keep only the coordinate z in the direction perpendicular to the surface. The distribution function $f(E, z)$ (suppressing spin and band indices for simplicity) describes the occupation of an electronic state $|E\rangle$ at the coordinate z . Electrons in state $|E\rangle$ are moving in different directions with a certain velocity distribution. In order to describe transport, it is necessary to use the velocity in z direction as an additional argument in the distribution function. It is now written as $f(E, z, v_z)$. Using Liouville's theorem, one can express the change in the number of electrons moving with a velocity v_z as:²⁶

$$\left. \frac{\partial f(E, z, v_z)}{\partial t} \right|_{\text{trans}} = -v_z \nabla_z f(E, z, v_z). \quad (8)$$

In the calculation of transport, we take into account the effect of inelastic electron-electron collisions on the distribution $f(E, z, v_z)$. In order to do this, we describe how both the electron-electron scattering rates from Eqs. (4–5) and the transport term from Eq. (8) are used in the Boltzmann equation for $f(E, z, v_z)$. We make the assumption that the velocity of the electrons after scattering is randomly distributed. The rate of change of $f(E, z, v_z)$ due to electrons scattering into and out of this state is then given by $\left. \frac{\partial f(E, z, v_z)}{\partial t} \right|_{\text{in}} = \left. \frac{\partial f(E, z)}{\partial t} \right|_{\text{in}}$ and $\left. \frac{\partial f(E, z, v_z)}{\partial t} \right|_{\text{out}} = \frac{f(E, z, v_z)}{f(E, z)} \left. \frac{\partial f(E, z)}{\partial t} \right|_{\text{out}}$, where the rates on the right hand side are calculated with Eqs. (4–5) using the velocity-averaged distribution $f(E, z) = (1/N_v) \sum_{i=1}^{N_v} f(E, z, v_z^{(i)})$. We use N_v discrete velocity intervals of width $\Delta v_z = (2v_F)/N_v$, neglecting the weak energy dependence of the velocity in the range of a few eV around E_F . These terms are used in the Boltzmann equation for $f(E, z, v_z)$ together with the terms for transport and optical excitation. The photoexcited electrons have a random distribution of velocities: $\left. \frac{\partial f(E, z, v_z)}{\partial t} \right|_{\text{optical}} = \left. \frac{\partial f(E, z)}{\partial t} \right|_{\text{optical}}$.

The transport effect is caused by the gradient in the particle density created by the photoexcitation within the optical penetration depth. We take into account the fact that sp and d electrons have different velocities due to their different degree of localization. The velocity of an electron in band α with wave vector k is given by $v_\alpha(k) = \frac{1}{\hbar} \frac{\partial E_\alpha(k)}{\partial k}$. Thus, nearly free electrons in sp -like bands have higher velocities (or smaller effective mass) than more localized electrons in flat, d -like bands. For s electrons, we take the Fermi velocity as the maximal velocity. For d electrons, we note that the velocity in is roughly proportional to the band width and we therefore set $v_d/v_s = W_d/W_s$. For all elements considered, we use $v_F = 18 \text{ \AA}/\text{fs}$ and $W_d/W_s = 0.4$.^{27,28} Thus, we distinguish between different elements purely by the relative contribution of sp and d electrons.

We have not included electron-phonon scattering into Eq. (2) because the time scale for energy transfer between electrons and phonons is on the order of ps and thus longer than the time scales considered in this work.²⁹ However, electron-phonon scattering provides an additional mechanism for momentum transfer and can thus reduce the efficiency of ballistic transport.³⁸ In our calculation, the neglect of electron-phonon scattering might lead to an overestimate of the transport effect. The inclusion of the momentum redistribution by electron-phonon scattering is beyond the scope of the present work, but will be the subject of a future publication.³⁰

In Eqs. (4–5), the transition rates are determined by the available phase space for a transition weighted by the square of the transition matrix element. Scattering out of an excited level and into an excited level are treated on the same footing. The two processes occur simultaneously because of energy conservation. The rate $\left. \frac{\partial f(E\sigma)}{\partial t} \right|_{e-e}^{\text{in}}$ for scattering into a level contains the effects leading to the refilling of the intermediate state. By calculating the scattering rates in a consistent manner for states above and below the Fermi energy, we keep track of the creation and relaxation of electrons as well as holes.

Note, from the Boltzmann equation we recover the Fermi-liquid behavior $\tau(E) \propto (E - E_F)^{-2}$ for the single-electron lifetime. To see this we write $\left. \frac{\partial f(E\sigma)}{\partial t} \right|_{e-e}^{\text{out}} = -\frac{f(E\sigma)}{\tau(E\sigma)}$ which yields $1/\tau(E\sigma) = 1/2 \int_{-\infty}^{\infty} dE' \{h_{E'\sigma} W(E\sigma, E'\sigma) + h_{E'\bar{\sigma}} W(E\sigma, E'\bar{\sigma})\}$ for the inverse lifetime. For simplicity now we take $\rho = \rho_\uparrow = \rho_\downarrow$ and $M^{\uparrow\uparrow} = M^{\downarrow\downarrow} = M$. Then the inverse lifetime reduces to

$$\frac{1}{\tau(E)} = \frac{2\pi}{\hbar} \int_0^E dE' \rho(E') \int_{-\omega}^0 d\varepsilon 2\rho(\varepsilon) \rho(\varepsilon + \omega) |M|^2, \quad (9)$$

where $\omega = E - E'$. One sees the influence of the DOS within the distance $(E - E_F)$ of the Fermi energy and of the Coulomb matrix element. For energies very close to E_F or for constant DOS ρ one obtains $1/\tau(E) = \frac{2\pi}{\hbar} \rho^3 |M|^2 (E -$

E_F)². Note, that the inverse lifetime is proportional to ρ^3 . In addition to the factor ρ from the relaxation of the initial electron at energy E , one also has to take into account the available phase space for the electron-hole pair created because of energy conservation, which yields a factor of ρ^2 . This may be compared with the FLT lifetime expression which is given by^{31,32} $\tau(E) = a_0(r_s)(E - E_F)^{-2}$, where $a_0(r_s) = 263r_s^{-5/2}$ fs eV² and r_s is the dimensionless parameter describing the density of the electron gas. It is given by the relation $1/n_e = 4\pi(r_s a_0)^3/3$, where n_e is the electron density and a_0 is the Bohr radius. Thus, the expression for $\tau(E)$ derived from $\left. \frac{\partial f(E\sigma)}{\partial t} \right|_{e-e}^{\text{out}}$ in the appropriate limit gives the same energy dependence as FLT.

One can try to understand the relaxation times observed in different metals by means of the FLT expression for τ by using r_s corresponding to the electron density in the metal. However, the expression is strictly valid only for free-electron-like metals and it is not simple to extend it to take into account d electrons. First one can use the electron density corresponding to sp electrons only. We take values for integrated sp and d electron densities of states in the solid from Ref. 33. The number of sp electrons per atom for Fe, Co, Ni, and Cu is 1.07, 1.13, 1.03 and 1.10, respectively. One obtains roughly $r_s \sim 2.6$ and $a_0 \sim 25$ fs eV² for all the metals Fe, Co, Ni, and Cu. This neglects d electrons altogether and does not yield any differences between these metals. On the other hand, if one uses the total number of sp and d electrons, one obtains values for r_s monotonically decreasing from $r_s = 1.32$ in Fe to $r_s = 1.22$ in Cu, leading to $a_0 = 130$ fs eV² for Fe and $a_0 = 161$ fs eV² for Cu. It is evident from the magnitude of a_0 that this overestimates the influence of d electrons. Clearly a more refined treatment is necessary which distinguishes between sp and d electrons and takes into account the DOS within a few eV of the Fermi energy. The influence of the d bands on the lifetime of a state depends on the distance E_d of the d bands to the Fermi energy: for small excitation energy $\Delta E = E - E_F < E_d$, the d bands should have little influence on the lifetime. In Sec. V, we will discuss the influence of d bands in more detail.

III. NUMERICAL RESULTS OF THE THEORY

To show clearly the influence of different physical mechanisms, the calculated relaxation times are presented in three steps including consecutively more processes in the calculation.

In the first step, we consider the single-electron lifetime. At this level, we take into account in the Boltzmann equation, Eq. (2), only scattering out of a particular level in addition to the optical excitation. Results are labelled by (*out*) in Figs. 3 and 5. After photoexcitation, the time evolution of the distribution function shows an exponential decay. The lifetime obtained in this way is a single-electron lifetime and can be compared with FLT or with lifetimes obtained from first-principles calculations of the self-energy.^{19,20} However, the single-electron lifetime is observed in an experiment only if there are no other effects present such as secondary-electron generation or transport. Thus, the calculated single-electron lifetime should not be directly compared with experimental results. It serves as a guide for comparison with other theoretical results and as a reference for comparison with results when secondary electrons and transport are included.

In the second step, we take into account secondary electrons, while neglecting transport effects. Thus, in the Boltzmann equation, we keep the scattering terms for scattering *into* and *out of* the levels. Results are labelled (*out, in*). The relaxation time obtained in this way includes effects of the whole distribution. Note, it is not a single-electron lifetime, but an effective relaxation time of the distribution.

In the third step, we also take into account transport effects. The loss of excited electrons due to transport out of the surface region will influence the occupation and hence the apparent electronic relaxation time. Results are labelled (*out, in, transport*).

The DOS for the different metals used as input in the calculation of the scattering rates in Eqs. (4–7) are taken from an FLAPW calculation³⁴ and are shown in Fig. 2. We distinguish only between d -like and sp -like states in the DOS. We take the partial d DOS from the calculation and use the remaining DOS as sp -like DOS. The total DOS are very similar to the ones given in Ref. 27. For Cu, however, we shift the d bands to lower binding energy by 0.4 eV in order to obtain agreement with ARPES results for the binding energy of the d bands.²¹ It is known that LAPW calculations might yield too small binding energies for the d bands.³⁵

The values for the optical penetration depth were obtained from the optical constants in Ref. 36. We use $\lambda_{\text{Fe}} = 124$ Å, $\lambda_{\text{Co}} = 108$ Å, $\lambda_{\text{Ni}} = 122$ Å, and $\lambda_{\text{Cu}} = 149$ Å for $h\nu = 3.0$ eV. For the range of photon energies considered, the energy dependence of the penetration depth can be neglected.

A. Numerical Results for Cu

Fig. 3 illustrates the effect of secondary electrons and transport on the intensity $I^{2\text{PPE}}$ (upper part) and relaxation time (lower part) for optical excitation with photon energy $h\nu = 3.3$ eV. The results for Cu show particularly clearly the influence of secondary electrons and transport. We use $M = 0.8$ eV and $|M^{\uparrow\uparrow}/M^{\uparrow\downarrow}| = 1$ for the Coulomb matrix elements. This choice will be justified at the end of this section.

In curve *a* of Fig. 3, we show $I^{2\text{PPE}}$ calculated from Eq. (1) without scattering and transport. In this case $I^{2\text{PPE}}$ is proportional to the number of optically excited (primary) electrons in the intermediate state. The optical excitation in Eq. (3) is proportional to the convolution of initial and final DOS, since we use constant optical transition matrix elements. The intensity shows an important contribution from initial states in the *d* band below $E - E_F = 1.3$ eV with a pronounced peak at 1.1 eV and a small contribution from initial states in the *s* band above 1.3 eV.

In curve *b* of Fig. 3, we show $I^{2\text{PPE}}$ keeping only the out-scattering term in Eq. (2), which corresponds to an exponential decay of the optically excited distribution. The intensity is reduced compared to the intensity without scattering, and the reduction gets stronger towards higher excitation energy due to the shorter lifetime. The relaxation time calculated in this way is a single-electron lifetime. For energies below $E - E_F = 2$ eV, it shows the energy dependence $\tau(E) \propto (E - E_F)^{-2}$ as in FLT. The FLT lifetime for Cu with $a_0 = 25$ fs eV² is shown by curve *e*. It is a factor of about 2.5 lower than the lifetime calculated using $M = 0.8$ eV.

In curve *c* of Fig. 3, we show the results using the in-scattering term as well as the out-scattering term in Eq. (2). At low energy a secondary-electron tail forms and the intensity becomes a superposition of the initial optical excitation and the secondary-electron tail. The relaxation time shown by curve *c* is an effective relaxation time of the distribution including secondary-electron effects. It is no longer monotonous and shows a distinct feature in the region of the intensity peak. We find a relative minimum at the position of the intensity peak. Further, the relative maximum corresponds to the *d*-band threshold above which very few optically excited *d* electrons are found. We can understand this by studying the contribution of secondary electrons. Comparing the intensities without (curve *b*) and with (curve *c*) secondary electrons, we find that in the region of the peak, the intensity is only slightly increased by secondary electrons, whereas it is strongly increased above the *d*-band threshold. This shows that in the intensity peak one observes mainly relaxation of optically excited electrons, whereas above the threshold, one finds mainly contributions of secondary electrons. Comparing the relaxation times, we find that in the region of the intensity peak and also at high energies $E - E_F > 2.5$ eV, the relaxation time with secondary electrons (curve *c*) comes very close to the relaxation time without secondary electrons (curve *b*), again showing that one observes mainly relaxation in these regions. Most secondary electrons are generated in the process of filling the holes in the *d* band created by the optical excitation (so-called Auger effect). The increase in the relaxation time is due to the fact that secondary electrons are generated with a certain delay after the optical excitation corresponding to the *d*-hole lifetime.^{10,37}

In Fig. 3 curve *d* shows the results obtained using transport in addition to secondary-electron effects. Compared to the case without transport (curve *c*), the intensity is reduced. The transport effect removes excited particles from the observation region close to the surface into the bulk and thus reduces the intensity. The relaxation time including transport (curve *d*) has a similar shape as the relaxation time with secondary-electron effects (curve *c*), but the magnitude of the relaxation time is strongly reduced by transport. Interestingly, curve *d* comes close to curve *b* in the region above the threshold ($E - E_F > 1.3$ eV). Thus, we find that for Cu in a certain energy range, the effects of secondary electrons and transport on the relaxation time roughly cancel. This has been pointed out in an analysis of a 2PPE experiment before.³⁸

Fig. 4 shows theoretical and experimental results for the 2PPE intensity and relaxation time for photon energies $h\nu = 3.0$ and 3.3 eV. Both the intensity peak and the relaxation time feature shift linearly with photon energy. As indicated by the dotted lines, the minimum in the relaxation time corresponds to the peak in the intensity, whereas the maximum in the relaxation time corresponds to the *d*-band threshold.

We have used a Coulomb matrix element $M = 0.8$ eV. With this choice we obtain at $E - E_F = 1$ eV for the single-electron lifetime $\tau = 55$ fs and for the relaxation time including secondary electron and transport effects $\tau = 40$ fs (for photon energy $h\nu = 3.3$ eV). The single-electron lifetime is in good agreement with first-principles calculations in the energy range $E - E_F < 2$ eV.¹⁹ It also yields good agreement with experimentally determined relaxation times at low energies ($E - E_F \approx 1$ eV).¹⁰ We remark that at higher energies ($E - E_F > 2$ eV), we would obtain better agreement with first-principles calculations and experiments for a smaller Coulomb matrix element $M = 0.6$ eV. Thus, the use of energy-dependent matrix elements might improve the overall agreement between theory and experiment over a wide energy range.

B. Numerical Results for Fe, Co, and Ni

First, we discuss numerical results shown in Figs. 5a and b and labelled by (*out*) for the single-electron lifetime in Fe, Co, and Ni. We use the same energy-independent Coulomb matrix element $M = 0.8$ eV and $|M^{\uparrow\uparrow}/M^{\uparrow\downarrow}| = 1$ for the different metals.

For constant and equal Coulomb matrix element M , the single-electron lifetime is directly related to the DOS shown in Fig. 2 and used as input for the calculation. The influence of the DOS on the lifetime is seen in the scattering-rate expression Eq. (4) or in the simplified expression Eq. (9). The scattering rate, the inverse of the lifetime, is proportional to a combination of terms which contain products of three factors of the DOS.

When comparing the single-electron lifetime of Cu shown in Fig. 3 (curve *b*) with the results in Fig. 5a for the transition metals, one can see that Cu has a lifetime much longer than the other metals. This is due to the small total DOS close to E_F . In Cu, the d bands are located about 2 eV below E_F and there is only a very small total DOS close to E_F (Fig. 2). The small d DOS close to E_F is due to hybridization with sp -like states. In Ni with one electron less than Cu, the d bands move closer to E_F . Furthermore, the d bands are split into a minority and majority spin band and a small portion of the minority d band is unoccupied, extending up to about 0.4 eV above E_F (Fig. 2). Due to the pronounced peak at the upper edge of the d -band, the minority DOS close to E_F is extremely large. This leads to a large phase space for electron-electron scattering at low energy. Thus at low energy (below $E - E_F = 1$ eV), Ni has the smallest calculated single-electron lifetime among the four elements. Co, with one electron less than Ni, has an even larger portion of unoccupied minority DOS, extending up to about 1.2 eV above E_F . Although the total number of unoccupied states is higher in Co than in Ni, the minority DOS at E_F is lower in Co. Thus at low energy (below 1 eV), Co has less phase space and the calculated lifetime is longer than in Ni. With increasing energy, more and more unoccupied states become available in Co, so that above 1 eV, the calculated lifetime in Co becomes shorter than the one in Ni. In Fe, again with one electron less compared to Co, the unoccupied minority DOS extends up to 2.4 eV above E_F , and even the majority DOS has a small unoccupied fraction. The minority DOS at E_F in Fe is lower than in Co and in Ni, so that Fe has the smallest phase space and the longest calculated lifetime at low energy.

Therefore, at low energy (below $E - E_F = 1$ eV), our simplified theory with equal M for the different metals gives $\tau_{\text{Ni}} < \tau_{\text{Co}} < \tau_{\text{Fe}}$. This trend changes for Co and Ni above 1 eV. Then we get $\tau_{\text{Co}} < \tau_{\text{Ni}}$. At even higher energy (above 2 eV, not shown in the figure), all of the unoccupied d states in Fe are available for a transition and one calculates $\tau_{\text{Fe}} < \tau_{\text{Co}} < \tau_{\text{Ni}}$. This relation is also observed in transmission experiments above the vacuum energy for electrons with energies above $E - E_F = 5$ eV.³⁹

In Fig. 5b the ratio of majority to minority single-electron lifetime $\tau_{\uparrow}/\tau_{\downarrow}$ is shown. For Co, this ratio is nearly constant with a value $\tau_{\uparrow}/\tau_{\downarrow} = 7.5$. This is understandable in view of the high and nearly constant ratio of minority to majority DOS at low energy. For Ni the ratio decreases from $\tau_{\uparrow}/\tau_{\downarrow} = 9.5$ at $E - E_F = 0.4$ eV to $\tau_{\uparrow}/\tau_{\downarrow} = 4$ at $E - E_F = 1.4$ eV. The decrease is due to the fact that above 0.4 eV there are no more unoccupied minority d states. The additional phase space gained by going to higher energy is the same for minority and majority electrons, leading to a smaller ratio. In Fe the ratio increases from $\tau_{\uparrow}/\tau_{\downarrow} = 0.5$ to 1 for excitation energies between $E - E_F = 0.4$ and 1.2 eV. Thus, majority electrons have a shorter calculated lifetime than minority electrons at low energy. This results from the unoccupied portion of the majority DOS above E_F , which for low energy leads to a larger phase space for the relaxation of majority electrons and therefore to a shorter lifetime.

Secondly, we discuss results shown in Figs. 5c and d obtained when secondary electrons are included in the calculation. They are labelled by (*out*, *in*). Transport effects are still neglected. The inclusion of secondary electrons leads to an increase of the relaxation time by a factor of about two as compared to the single-electron lifetime. The strongest effect is found at the lowest energies. The increase is stronger for the elements with the shortest calculated lifetimes (Ni, Co), so that the differences in the relaxation time including secondary electrons between Ni, Co, and Fe are smaller than for the single-electron lifetime. The ratio $\tau_{\uparrow}/\tau_{\downarrow}$ for Ni and Co is reduced to $\tau_{\uparrow}/\tau_{\downarrow} = 4 - 5$ for Ni and $\tau_{\uparrow}/\tau_{\downarrow} = 5 - 6$ for Co. For Fe, the ratio is nearly unchanged, $\tau_{\uparrow}/\tau_{\downarrow} = 0.5 - 1$. The reduction of the ratio $\tau_{\uparrow}/\tau_{\downarrow}$ due to secondary electrons is understandable in view of the fact that the inclusion of secondary electrons leads to a coupling between majority and minority electron populations via electron-electron scattering. Relaxing minority electrons can excite majority electrons and vice versa. For Co and Ni, for example, longer-living majority electrons will continue to excite minority electrons after the shorter-living primary minority electrons have relaxed. The apparent minority-electron relaxation time becomes longer and the ratio $\tau_{\uparrow}/\tau_{\downarrow}$ becomes smaller by this process. The trends among the calculated relaxation times of the transition metals, particularly the relation $\tau_{\text{Ni}} < \tau_{\text{Co}} < \tau_{\text{Fe}}$ at $E - E_F < 1$ eV are unchanged when secondary electrons are included.

The spectral shape of the optical excitation, i.e. the distribution of primary electrons, has some influence on the calculated relaxation time. For example, electrons excited to a high energy lead to more secondary electrons (due to the short lifetime of the primary electrons) and to a distribution extending to higher energy (due to the high energy of the primary electrons). Similar arguments apply to the energetic position of the holes created by the optical

excitation. The results for the transition metals shown in Fig. 5 are obtained using an optical excitation with photon energy $h\nu = 3.0$ eV and constant optical transition matrix elements in Eq. (3). We have also studied the effect of a different optical excitation on the relaxation time. We have modelled a resonant optical excitation where excitations take place dominantly between an initial state at the top of the d band and a final state in the sp band. No significant difference in the calculated relaxation time for the two different shapes of the excitation is obtained.

Thirdly, we discuss results of the calculations including transport in addition to secondary-electron effects in the Boltzmann equation, Eq. (2). They are labelled by (*out, in, transport*). Results are shown in Figs. 5e and f. The inclusion of transport leads only to a very slight reduction of the effective relaxation time in Fe, Co, and Ni. The ratio $\tau_{\uparrow}/\tau_{\downarrow}$ as well is only slightly affected by transport. This is in contrast to the strong reduction of the effective relaxation time in Cu (compare curves *c* and *d* in Fig. 3). The explanation is that the typical transport relaxation timescale is about 40 fs.^{4,10} This is shorter than, or comparable to, the single-electron lifetime in Cu in the energy range considered, but considerably longer than the typical lifetimes in Fe, Co, or Ni. Thus, transport is expected to have great influence for Cu, but not for the transition metals.

IV. EXPERIMENT

A. TR-2PPE technique

The TR-2PPE pump-probe experiments are carried out in a UHV chamber by monitoring the number of electrons at a given kinetic energy as a function of the delay between the pump and probe pulses. We employ the equal-pulse correlation technique, i.e. the two pulses are monochromatic and equal in intensity, but cross-polarized. For metals, the use of orthogonal linear polarized light pulses suppresses coherent interference effects (within the limit of rapid dephasing) to a large extent.⁴ Otherwise they influence the optical transition process and would make the reconvolution of the raw data much more difficult. Furthermore, the influence of Cs-induced surface states on the lifetime can be suppressed (see below).

The non-linearity of the two-photon process leads to an increase in the 2PPE yield when the pulses are spatially and temporarily superimposed. As long as the two laser pulses temporarily overlap it is obvious that an electron can be emitted by absorbing just one photon from each pulse. However, if the pulses are temporarily separated, then an excited electron from the first pulse is able to absorb a photon from the second pulse but only as long as the inelastic lifetime of the intermediate state exceeds the delay or the normally unoccupied electronic state is refilled by a secondary electron. Due to a precise measurement of the time delay between the two pulses (1 fs $\hat{=}$ path length difference of 0.3 μm), this technique allows us to analyze relaxation times which are considerably shorter than the laser pulse duration.

We use laser pulses at low fluence and peak power to avoid space-charge effects or highly excited electron distributions. We emphasize that the count rate is much lower than one electron per pulse. Therefore, we measure the relaxation and transport of individual excited electronic states rather than the collective behavior of transiently heated non-equilibrium distribution. We have to roughly calculate the fraction of excited electrons. Typically, we have a laser fluence of about 0.3 nJ/pulse in each beam resulting in 6×10^8 photons per pulse. For a spot size of ~ 150 μm and a penetration depth of the blue light of ~ 150 \AA , the volume in which the laser light will be absorbed is about 3×10^{-10} cm^3 . If 10% of the light is absorbed by the metal, then 6×10^7 photons are absorbed by 7×10^{13} atoms which results in a fractional excitation of roughly 1 part in 10^6 .

B. Experimental set-up

A schematic overview of the experimental set-up is shown in Fig. 6. The samples are mounted in a UHV chamber with a base pressure in the 10^{-11} mbar range. It is equipped with a cylindrical sector electron energy analyzer (CSA) and a spin analyzer, based on spin-polarized low-energy electron diffraction (SPLEED).⁴⁰ The earth's magnetic field is shielded by μ -metal coverings inside the chamber. Standard surface-physics methods such as Auger-electron spectroscopy (AES) and low-energy electron diffraction (LEED) are available to check the cleanliness and the surface structure of the samples. The orientation of the samples is 45° with respect to the laser beam and the electrons are detected in normal-emission geometry. Remanent magnetization of the ferromagnetic samples is achieved by a magnetic field pulse from a coil. The geometric arrangement of the spin analyzer allows the measurement of the spin polarization along the horizontal in-plane axis of the sample. To minimize the effects of stray fields and to facilitate electron collection, a bias voltage (-4 V for Cu and -15 V for Ni, Co, and Fe) is applied between the sample and the CSA. For spin-resolved measurements the electrons are guided into the SPLEED analyzer, which is located on top of

the CSA. In this spin analyzer the electrons are first accelerated to 104.5 eV kinetic energy, as the highest figure of merit for this kind of analyzer is known to be at this primary-electron energy.⁴⁰ Thereafter, the electrons are scattered at a tungsten (001) crystal. From the resulting LEED feature, the (-2,0) and (2,0) electron beams that have a high spin asymmetry, are counted in two different channeltrons. The Sherman factor S , a quantity for the spin selectivity of an analyzer, is found to increase from 0.2 to 0.25 over the two years of operation; the highest value was reached after having the tungsten SPLEED crystal a long period in very low pressure.

The time-resolved 2PPE experiments are performed with a femtosecond mode-locked Ti:sapphire laser, pumped by about 10 W from a cw Ar⁺ laser. The system delivers transform-limited and sech² temporal shaped pulses of up to 9 nJ/pulse with a duration of 40 fs at a repetition rate of 82 MHz. The linearly polarized output of the Ti:Sapphire laser is frequency-doubled in a 0.2 mm thick Beta Barium Borate (BBO) crystal to produce UV pulses at $h\nu = 3$ to 3.4 eV. The UV beam is sent through a pair of prisms to pre-compensate for pulse broadening due to dispersive elements like lenses, beamsplitters and the UHV-chamber window in the optical path. A GVD and intensity-loss matched interferometric autocorrelator set-up is used for the pump-probe experiment (see Fig. 6). The pulses are split by a beamsplitter to equal intensity (pump and probe pulses), and one path is delayed with respect to the other by a computer-controlled delay stage. Both beams are combined co-linearly but cross-polarized by a second beamsplitter and are focused at the sample surface.

For the ferromagnetic samples, we use evaporated films because they can be held magnetized in a single-domain state without an applied external field and the stray field is much smaller compared to a bulk ferromagnet. In principle, this experiment could also be performed with bulk samples. The ferromagnetic films are evaporated onto a Cu(001) substrate in a separable chamber. We use a water-cooled evaporator based on electron-beam heating. The material to be evaporated (of 99.999% purity) was inside a molybdenum crucible (Co, Fe) or directly evaporated from a 1 mm thick wire (Ni). The evaporation rate (around 0.2 nm/min) was checked with a quartz oscillator, which is calibrated against atomic-force-microscope thickness measurements. During evaporation the pressure remained in the 10^{-10} mbar region.

The thickness of the ferromagnetic films must fulfill the following requirements. Firstly, it has to be large enough, in order to avoid an influence of electrons from the Cu substrate. Secondly, it should be possible to remanently magnetize the film by a suitable strong field pulse. And thirdly, the axis of the magnetization has to lie in the film plane because the geometry of our spin analyzer only allows the measurement of transversally polarized electrons.

Cobalt films, epitaxially grown on Cu(001) surfaces, are formed in a stable fcc structure and exhibit in-plane magnetization. For thick films, the in-plane magnetization easy axis lies along the (110) direction of the Cu crystal.⁴¹ In-plane magnetization was detectable starting at a thickness of around 0.4 nm. This is in agreement with other investigations using the magneto-optical Kerr effect.⁴² Above a film thickness of 2 nm, the spin polarization did not increase any more on further deposition of Co. For our investigations we evaporated 10 nm thick Co films.

Iron grows in the fcc structure on Cu(001) during the initial steps of evaporation. The magnetization vector is oriented perpendicular to the film surface. Above a thickness of around 2 nm a bcc (110) structure starts developing.⁴³ The magnetic easy axis for these thick films is found to lie parallel to the Cu(100) axis.⁴⁴ We use 20 nm thick iron films for our investigation.

For Ni on Cu(001) the magnetization vector is in-plane for small thicknesses, then it switches to out-of-plane at a thickness of around 1.2 nm.⁴⁵ Only at larger thicknesses of around 6-7 nm does it turn back to in-plane.⁴⁶ We found a saturation of the spin polarization for thicknesses above 25 nm. Therefore, we evaporated 40 nm thick Ni films for our measurements.

The clean metal surfaces are first dosed with Cs to lower the surface work function, a well-known technique. This enabled lifetime measurements of lower excited states, increasing the useful energy range of the spectra closer to the Fermi energy (see Fig. 1). Cs is evaporated from a thoroughly out-gassed getter source (SAES). The effect on the lifetime by dosing a metal surface with small amount of Cs (<0.1 ML) has been thoroughly investigated in the last years.^{47,48} Using cross-polarized pulses no differences in the lifetime have ever been found between a clean and a cesiated metal surface by means of TR-2PPE.⁴⁹ In addition, we found no differences in spin polarization between the clean and the cesiated surfaces in the overlapping energy region between 1.7 and 3.3 eV.

C. Experimental results for Cu

In Fig. 4b the extracted relaxation time as a function of the intermediate-state energy for a Cu(111) surface is shown, using a photon energy of 3.0 eV (\square) and 3.3 eV (\circ). The data are reconvoluted from the experimentally obtained cross-correlation traces using a rate-equation model for the population of the intermediate state. In the case of rapid dephasing, and assuming an exponential depletion of the nascent photoexcited electron population, the evolution of the transient population $N^*(t)$ of the intermediate state is given by $dN^*(t)/dt = A(t) - N^*(t)/\tau$

where $A(t)$ is the excitation induced by the first (pump) laser pulse. Details of the way to extract the relaxation time from the measured signal have been given in previous publications.^{1,4,10} As expected, the lifetime increases as the excited state energy decreases, caused by the reduced phase space for electron-electron scattering (see Secs. II, III A, and Fermi-liquid theory). However, at an intermediate-state energy, where the intensity becomes dominated by interband transition from the d band to the unoccupied sp band (strong d -band peak in the intensity), the measured relaxation time decreases by more than a factor of two before it increases again. By changing the photon energy from $h\nu = 3.0$ eV to $h\nu = 3.3$ eV, both the d -band peak in the intensity and the dip in the measured lifetime move with the same energy difference $\Delta E = \Delta h\nu$ as expected. The striking difference in the values observed in the energy range $E - E_F = 0.7 - 1.3$ eV indicate quite clearly that the relaxation time can depend critically on the used photon energy.

D. Experimental results for Fe, Co, and Ni

1. Spin-integrated time-resolved 2PPE measurements

We used the same equal-pulse correlation technique to extend the investigation of the hot-electron relaxation to transition metals Co, Fe, and Ni. Compared with noble metals, in which the d shell is completely filled (see Cu and Ag), the d band of transition metals is only partially filled, and the electronic and relaxation properties are dominated to a considerable degree by these d electrons. The strong localization of these d electrons results in a narrower band and hence in a much higher DOS near the Fermi level as compared with the sp electrons in Cu and Ag. A higher density of occupied and unoccupied states near the Fermi level is expected to lead to faster relaxation and hence to a shorter inelastic lifetime of excited electronic states as discussed in Sec. III B. This prediction is well satisfied by our data. Fig. 7 shows a comparison of the extracted relaxation time of silver and the three investigated ferromagnetic transition metals cobalt, nickel and iron. The experimental values for these metals are at least a factor of 10 smaller than those of Cu and Ag. These small values reduce the energy range in the region of 0.3 eV to 1.3 eV which provides a meaningful statement about the relation in the relaxation time between the three investigated transition metals. In contrast to the numerical results calculated using the same Coulomb matrix element M for different metals (see Sec. III B), the data indicate a relation $\tau_{\text{Fe}} < \tau_{\text{Ni}} < \tau_{\text{Co}}$ within this energy range.

2. Spin- and time-resolved 2PPE measurements

Adding a spin analyzer to the CSA energy analyzer makes possible the separate but simultaneous measurement of both spin states. The electrons of a fixed energy are counted according to their spin in two different channeltrons as a function of the time delay between the two pulses, at a given magnetization direction. To compensate for an apparatus-induced asymmetry, the magnetization is then reversed and the measurement is taken again. From the resulting four datasets the relaxation times τ_{\uparrow} and τ_{\downarrow} for spin-up and spin-down electrons are extracted by using the same deconvolution method as discussed above. Each pair of data points presented in the plots of this section is the average of eight to ten single relaxation time measurements.

The spin dependence will have a superimposed effect on the spin-integrated relaxation time. Therefore, a spin dependence in the relaxation time can only be resolved if there is already a certain relaxation time detectable with spin-integrated measurements. As shown in Fig. 7, in the energy range above 1.4 eV, we find for all three transition metals a relaxation time smaller than our time resolution (< 2 fs). On the other hand, at intermediate-state energies close to E_F , the electrons emitted by 1PPE processes start becoming important. They induce a large background to the 2PPE signal and make an accurate extraction of the lifetimes difficult. Therefore, spin-resolved measurements can only be usefully performed for intermediate-state energies between 0.3 and 1.1 eV.

In Fig. 8 the spin-dependent relaxation time for electrons (upper part) and the ratio of majority to minority lifetime (lower part) of Fe, Co, and Ni films are plotted. The error bars in the plot represent the statistical scatter. The experimental results of the three examined ferromagnetic materials show two common facts: i) The lifetime for majority-spin electrons is always found to be longer than the lifetime for minority-spin electrons and ii) the value for $\tau_{\uparrow}/\tau_{\downarrow}$ was found to lie between 1 and 2. The largest differences between τ_{\uparrow} and τ_{\downarrow} are found for Ni and Co, whereas for Fe, the difference is slightly reduced. This qualitative behavior of the spin-dependent lifetime can be readily explained by the excess of unfilled minority-spin states compared to unfilled majority-spin states. According to this simple model, the spin dependence of the scattering rate is larger for the strong ferromagnets Co and Ni than for the weak ferromagnet Fe. This is in agreement with our measurements, where only a small spin effect could be detected for Fe. In Fe, this model would even predict a reversal of the effect for low energies below 1 eV, i.e. the lifetime for spin-down electrons should become longer than the lifetime for spin-up electrons, see Fig. 5b. A ratio of majority to minority

relaxation time R below 1 is, however, not observed for $E - E_F < 1$ eV. This result indicates that the simple model, considering the different number of empty electronic states as the only decisive factor for a spin-dependent relaxation time, is not sufficient for a quantitative interpretation of our experimental data.

V. DISCUSSION

First, in Fig. 4 we compare experimental and theoretical results for Cu for photon energies $h\nu = 3.0$ and 3.3 eV. Experimental and theoretical results show qualitative agreement regarding the main features. The peak in the intensity and the feature in the relaxation time (relative minimum and maximum) shift linearly with photon energy. The minimum in the relaxation time corresponds to the peak in the intensity and the maximum in the relaxation time corresponds to the d -band threshold. The explanation that the feature in the calculated relaxation time is due to the secondary electrons was given in detail in Sec. III A. The good agreement between calculated and experimental results is a strong evidence for this explanation. The calculations reproduce the features observed in different experiments^{8–10} in a natural way by including secondary electrons without invoking further explanations such as excitonic states involving $3d$ electrons.⁹ The differences between theoretical and experimental results in Fig. 4 lead to several conclusions. Both the peak in the intensity and the difference between the minimum and maximum of the relaxation time are more pronounced in the experiment than in the calculation. This may be an evidence that the calculation yields too many secondary electrons which cause a too strong background and thus a too small structure in the 2PPE intensity (see the upper part of Fig. 4a). The relatively small increase from the minimum to the maximum in the calculated relaxation time should not be affected much by this, but may rather point to the fact that the lifetime of the d holes in the calculation is too small. Note, due to the large d DOS below E_F , there is no symmetry between hole lifetimes and lifetimes of excited electrons. In our calculations, hole lifetimes for energies below the d -band threshold are very short due to the large DOS. If the hole lifetimes were larger, then fewer secondary electrons would be generated, but with a longer delay after the creation of the electron-hole pair by the laser pulse. A longer delay will lead to the observation of a longer relaxation time in the excited state when secondary-electron contributions are important.

The interpretation given here that the non-monotonous feature in the lifetime in Cu is due to secondary (Auger) electrons has raised some controversy in the literature.^{8–10,12,13} While Knoesel *et al.*¹⁰ interpret their data by contributions from Auger electrons at intermediate-state energies above the d -band peak, Petek *et al.*¹³ argue that secondary electrons make no significant contribution to the signal above $E - E_F = 1.5$ eV (for photon energy $h\nu = 3.1$ eV). The argument is based on a temperature-dependent delayed rise in the 2PPE signal as a function of time delay between the laser pulses, which is observed below and immediately above the d -band peak at $E - E_F = 0.9$ eV, but which vanishes above $E - E_F = 1.5$ eV and in the region of the peak. The temperature-dependent delayed rise is interpreted as a contribution from Auger electrons, which agrees with our interpretation of the feature in the lifetime. In Ref. 13, the fact that the delayed rise vanishes above 1.5 eV is taken as evidence that Auger electrons are absent in this energy region. In contrast to this conclusion, our calculations show significant contributions from secondary electrons up to about $E - E_F = 2.5$ eV (compare the relaxation times without [curve *b*] and with [curve *c*] secondary electrons in Fig. 3). We argue in the following that the absence of a resolvable second peak in the 2PPE signal is no evidence for the absence of Auger electrons. Thus the results of Ref. 13 are not in contradiction with our results. One would observe a second peak with a delay given by the hole lifetime at the d -band peak if all Auger electrons were created at a fixed rate corresponding to this hole lifetime. However, Auger electrons are also created by the filling of holes deeper in the d band with energies up to $h\nu$. These deep holes have shorter lifetimes than the ones at the top of the d band. Thus they lead to secondary-electron contributions to the dynamics in the intermediate state with a smaller delay time. The fact that holes with different lifetimes contribute to the secondary-electron dynamics makes it difficult to observe a resolvable second peak with a fixed delay corresponding to the lifetime at the d -band peak. Thus in our view, the measurements reported in Refs. 12,13 are not in contradiction with the interpretation of the non-monotonous feature in the relaxation time given by us and in Ref. 10.

In Figs. 9 and 10 we compare experimental and theoretical results for the spin-averaged relaxation time τ and the ratio $\tau_\uparrow/\tau_\downarrow$ of majority and minority relaxation time for the ferromagnetic transition metals Fe, Co, and Ni. The discrepancies between experimental and theoretical results indicate that both DOS and Coulomb matrix elements play a role. Note, theoretical results refer to relaxation times of the distribution including secondary-electron effects. Transport effects have been neglected here in view of the fact that they cause only minor changes in the relaxation time of the transition metals, see Fig. 5.

First, the results calculated with $M = 0.8$ eV for all the transition metals are shown by the curves *a* in Figs. 9 and 10. The difference in the calculated relaxation times for Fe, Co, Ni, and Cu is then only due to the different DOS used as input for the calculation. Note, the calculated relaxation time is smaller than the experimental one in Co and Ni, while it is larger in Fe. The calculated ratio $\tau_\uparrow/\tau_\downarrow$ is larger in Co and Ni than the experimental one, but it is

smaller in Fe.

Secondly, in curves *b*, we show results of calculations using again $M = 0.8$ eV, but the reduced value $|M^{\uparrow\uparrow}/M^{\uparrow\downarrow}| = 0.5$. One expects that the matrix element $M^{\uparrow\uparrow}$ for scattering of parallel spins is smaller than $M^{\uparrow\downarrow}$ for antiparallel spins, since electrons with parallel spins avoid each other due to the Pauli exclusion principle.⁵⁰ The ratio $\tau_{\uparrow}/\tau_{\downarrow}$ is strongly reduced in Co and Ni, while it is increased in Fe, which leads to satisfactory agreement for $\tau_{\uparrow}/\tau_{\downarrow}$ between experimental and theoretical results. The spin-averaged relaxation time is not strongly affected by the value of $|M^{\uparrow\uparrow}/M^{\uparrow\downarrow}|$.

Thirdly, we take into account different Coulomb matrix elements M for the various metals, while we still use $|M^{\uparrow\uparrow}/M^{\uparrow\downarrow}| = 0.5$. The results are given by the curves *c* in Figs. 9 and 10. For Co and Ni we use $M = 0.4$ eV, while for Fe we take $M = 1.0$ eV. The use of these values for M leads to reasonable agreement between theoretical and experimental results for both the spin-averaged relaxation time and the ratio $\tau_{\uparrow}/\tau_{\downarrow}$.

Different Coulomb matrix elements in Fe, Co, Ni, and Cu are mainly caused by the influence of d electrons. Note, while in isolated atoms, Coulomb matrix elements do not vary much from Cu to Fe,⁵¹ in solids the band character, the position of the d band, and the screening of d electrons are expected to change this. The screened Coulomb matrix elements for scattering between Bloch states with wave vectors \mathbf{k}_i in bands α_i is given by

$$M_{3;4}^{1;2} = \int d^3r d^3r' \psi_{\mathbf{k}_1\alpha_1}^*(\mathbf{r})\psi_{\mathbf{k}_2\alpha_2}^*(\mathbf{r}') \frac{e^2}{\varepsilon(|\mathbf{r} - \mathbf{r}'|, \omega) |\mathbf{r} - \mathbf{r}'|} \psi_{\mathbf{k}_3\alpha_3}(\mathbf{r})\psi_{\mathbf{k}_4\alpha_4}(\mathbf{r}'). \quad (10)$$

Here, ε is the dielectric function. The Coulomb matrix elements are of course influenced by d electrons, since their wave functions are more localized and also since they contribute to the screening of the Coulomb potential. The strong localization of d electrons leads to smaller overlap with sp -electron wave functions and therefore to smaller transition matrix elements when $sp \rightarrow d$ transitions are involved as compared to matrix elements involving $sp \rightarrow sp$ transitions. Note, the d -electron wave functions get more localized from Fe to Cu. The additional screening of d electrons is contained in the dielectric function $\varepsilon(|\mathbf{r} - \mathbf{r}'|, \omega)$, where ω is the energy transferred in the transition. Somewhat depending on ω , d electrons closer to the Fermi energy contribute mainly to screening. In the static limit ($\omega \rightarrow 0$), the Lindhard dielectric function for a free electron gas reduces to $\varepsilon(q) = 1 + k_0^2/q^2$ such that the screened Coulomb interaction in real space takes the form $V(r) = \frac{e^2}{r} e^{-k_0 r}$. In the Thomas-Fermi approximation, the screening wave vector is directly related to the DOS at the Fermi level,²⁶ $k_0 = 4\pi e^2 \rho(E_F)$. In the case of transition metals, the expressions are not strictly valid because d electrons are not free-electron-like. Although the quantitative contribution of d electrons to screening is not well-known, qualitatively it is clear that a higher DOS near the Fermi level leads to stronger screening. This may explain that the screened Coulomb matrix element in Co and Ni with many d electrons close to the Fermi energy is smaller than the one in Cu with nearly no d electrons close to the Fermi energy. For larger energy transfer ω , also electrons further away from the Fermi energy contribute to screening. Then ultimately the total number of d electrons influences screening. This could be the reason why Fe, which has fewer d electrons, has a larger Coulomb matrix element than Co, Ni, and Cu.

After completion of our study we became aware of related work about the influence of d electrons on the lifetime of low-energy electrons in noble and transition metals.^{17,19,20} Choosing different matrix elements for sp and d states, Zarate *et al.*¹⁷ obtain good agreement with experimental results for Co.¹⁴ Campillo *et al.*¹⁹ and Schöne *et al.*²⁰ have calculated lifetimes in Cu using the density-functional theory for the determination of the electronic structure and have found important contributions of d electrons to the lifetime via screening, localization of the wave function and DOS effects.

VI. CONCLUSION

We have presented experimental and theoretical results for the dynamics of excited electrons in Cu, Fe, Co, and Ni.

The results for Cu show the influence of secondary electrons and transport effects on the observed relaxation time. The non-monotonous behavior in the relaxation time obtained in the calculation is in qualitative agreement with experiments. It seems desirable to achieve a better quantitative agreement for this structure in order to draw definitive conclusions about the role played by secondary electrons.

Experimental results for the spin-dependent relaxation time for Fe, Co, and Ni reveal that $\tau_{\text{Fe}} < \tau_{\text{Ni}} < \tau_{\text{Co}}$ and that $\tau_{\uparrow}/\tau_{\downarrow}$ lies between 1 and 2 for the three metals.

The comparison of experimental and theoretical results shows that DOS effects alone do not explain the magnitude of the relaxation time for the various transition metals observed in experiments. The differences between the calculation using the same Coulomb matrix element for Fe, Co, and Ni and experiments reveal that Coulomb-matrix-element effects are important.

As an outlook for further studies, we conclude that more detailed calculations have to include a first-principles calculation of the Coulomb interaction matrix elements. Notably one has to take into account the screening by

the d electrons, the influence of the localized d -electron wave functions on the Coulomb matrix elements, and the energy dependence of the matrix elements. Further studies of the influence of the optical excitation, for example the influence of the photon energy and the polarization of the incoming light on the observed dynamics, are needed. Also the influence of the hole lifetime on the calculated relaxation times should be investigated. The rate of filling of d -band holes influences the time evolution of the distribution and hence also the observed relaxation time for levels above the Fermi energy via the generation of secondary electrons. Hole lifetimes have been observed in recent experiments on Cu,⁵² and their effect on two-photon photoemission has also been considered in a recent theoretical work.¹¹

ACKNOWLEDGMENTS

R.K. and K.B. acknowledge financial support by Deutsche Forschungsgemeinschaft (SFB 290). We wish to thank J. Dewitz for providing results of band-structure calculations and C. Timm and G. Bouzerar for interesting discussions. R.B. and M.A. would like to thank all co-workers who contributed to the experimental work described here, in particular M. Bauer, S. Pawlik, W. Weber, and D. Oberli. H.C. Siegmann is thanked for many stimulating discussions.

APPENDIX A: DETERMINATION OF THE RELAXATION TIME

In order to determine the effective relaxation time, we fit the occupation function calculated from Eq. (2) with a function f describing exponential decay with a relaxation time τ obtained from the equation: $\frac{\partial f}{\partial t} = \frac{\partial f}{\partial t}\Big|_{\text{optical}} - \frac{f}{\tau}$. The fit to the occupation calculated from Eq. (2) is done by taking τ for which f has the maximum at the same time. The comparison of the curves in Fig. 11 shows that this is a valid procedure over a wide range of energies, even where secondary electrons dominate (see $E - E_F = 0.8$ or 1.3 eV). The fact that the deviations are very small shows that although the calculated curves do not exactly show exponential behavior, they can be fitted well by a curve f showing exponential decay for some effective relaxation time.

APPENDIX B: ELECTRON-ELECTRON SCATTERING RATES

The scattering rate out of the state with momentum \mathbf{p} , band α (designating sp or d -like wave function) and spin σ is given in first order time-dependent perturbation theory (golden rule) by:

$$\begin{aligned} \left. \frac{\partial f_{\mathbf{p}\alpha\sigma}}{\partial t} \right|_{e-e}^{\text{out}} &= -f_{\mathbf{p}\alpha\sigma} \frac{2\pi}{\hbar} \sum_{\mathbf{p}'\mathbf{k}\mathbf{k}',\beta\gamma\delta} \left\{ \frac{1}{2} f_{\mathbf{k}\gamma\sigma} (1 - f_{\mathbf{p}'\beta\sigma}) (1 - f_{\mathbf{k}'\delta\sigma}) \left| M_{\mathbf{p}'\beta\sigma; \mathbf{k}'\delta\sigma}^{\mathbf{p}\alpha\sigma; \mathbf{k}\gamma\sigma} - M_{\mathbf{k}'\delta\sigma; \mathbf{p}'\beta\sigma}^{\mathbf{p}\alpha\sigma; \mathbf{k}\gamma\sigma} \right|^2 \right. \\ &\quad \times \delta(E_{\mathbf{p}\alpha\sigma} + E_{\mathbf{k}\gamma\sigma} - E_{\mathbf{p}'\beta\sigma} - E_{\mathbf{k}'\delta\sigma}) \\ &\quad + f_{\mathbf{k}\gamma\bar{\sigma}} (1 - f_{\mathbf{p}'\beta\sigma}) (1 - f_{\mathbf{k}'\delta\bar{\sigma}}) \left| M_{\mathbf{p}'\beta\sigma; \mathbf{k}'\delta\bar{\sigma}}^{\mathbf{p}\alpha\sigma; \mathbf{k}\gamma\bar{\sigma}} \right|^2 \\ &\quad \left. \times \delta(E_{\mathbf{p}\alpha\sigma} + E_{\mathbf{k}\gamma\bar{\sigma}} - E_{\mathbf{p}'\beta\sigma} - E_{\mathbf{k}'\delta\bar{\sigma}}) \right\}. \end{aligned} \quad (\text{B1})$$

In the same manner, one defines the scattering rate $\left. \frac{\partial f_{\mathbf{p}\alpha\sigma}}{\partial t} \right|_{e-e}^{\text{in}}$ for scattering into a state. The first and second terms describe scattering between electrons of the same and of opposite spin, respectively.

Sums over momenta are converted into integrals over energies in the random- \mathbf{k} approximation.¹⁶ The conversion to \mathbf{k} -averaged quantities is done in the following way:

$$\sum_{\mathbf{k}} f_{\mathbf{k}\alpha\sigma} \rightarrow \int_{-\infty}^{\infty} dE \rho_{E\alpha\sigma} f_{E\alpha\sigma}.$$

Each \mathbf{k} sum leads to a factor of the DOS, $\rho_{E\alpha\sigma}$. Products of distribution functions and densities of states are defined as $e_{E\alpha\sigma} = \rho_{E\alpha\sigma} f_{E\alpha\sigma}$ and $h_{E\alpha\sigma} = \rho_{E\alpha\sigma} (1 - f_{E\alpha\sigma})$ and designate the number of electrons and holes. The random- \mathbf{k} approximation allows the replacements $\mathbf{p} \rightarrow E$, $\mathbf{p}' \rightarrow E'$, $\mathbf{k} \rightarrow \varepsilon$ and $\mathbf{k}' \rightarrow \varepsilon'$. The integral over ε' can be performed because of the δ -function and allows to replace ε' by $\varepsilon + \omega$ with $\omega = E - E'$. The \mathbf{k} -averaged expressions for the scattering rates out of and into the state $E\alpha\sigma$ are then given by:

$$\left. \frac{\partial f_{E\alpha\sigma}}{\partial t} \right|_{e-e}^{\text{out}} = -f_{E\alpha\sigma} \frac{1}{2} \sum_{\beta} \int_{-\infty}^{\infty} dE' \left\{ h_{E'\beta\sigma} W(E\alpha\sigma, E'\beta\sigma) + h_{E'\beta\bar{\sigma}} W(E\alpha\sigma, E'\beta\bar{\sigma}) \right\}, \quad (\text{B2})$$

$$\left. \frac{\partial f_{E\alpha\sigma}}{\partial t} \right|_{e-e}^{\text{in}} = (1 - f_{E\alpha\sigma}) \frac{1}{2} \sum_{\beta} \int_{-\infty}^{\infty} dE' \left\{ e_{E'\beta\sigma} W(E'\beta\sigma, E\alpha\sigma) + e_{E'\beta\bar{\sigma}} W(E'\beta\bar{\sigma}, E\alpha\sigma) \right\}. \quad (\text{B3})$$

with the definitions

$$W(E\alpha\sigma, E'\beta\sigma) = \frac{2\pi}{\hbar} \sum_{\gamma\delta} \int_{-\infty}^{\infty} d\varepsilon \left(e_{\varepsilon\gamma\sigma} h_{\varepsilon+\omega, \delta\sigma} \left| M_{E'\beta\sigma; \varepsilon+\omega, \delta\sigma}^{E\alpha\sigma; \varepsilon\gamma\sigma} - M_{\varepsilon+\omega, \delta\sigma; E'\beta\sigma}^{E\alpha\sigma; \varepsilon\gamma\sigma} \right|^2 \right. \\ \left. + e_{\varepsilon\gamma\bar{\sigma}} h_{\varepsilon+\omega, \delta\bar{\sigma}} \left| M_{E'\beta\sigma; \varepsilon+\omega, \delta\bar{\sigma}}^{E\alpha\sigma; \varepsilon\gamma\bar{\sigma}} \right|^2 \right), \quad (\text{B4})$$

$$W(E\alpha\sigma, E'\beta\bar{\sigma}) = \frac{2\pi}{\hbar} \sum_{\gamma\delta} \int_{-\infty}^{\infty} d\varepsilon e_{\varepsilon\gamma\bar{\sigma}} h_{\varepsilon+\omega, \delta\sigma} \left| M_{\varepsilon+\omega, \delta\sigma; E'\beta\bar{\sigma}}^{E\alpha\sigma; \varepsilon\gamma\bar{\sigma}} \right|^2. \quad (\text{B5})$$

For the calculation, we will use a simple parametrization of the matrix elements. First, we do not further distinguish between states of *sp* or *d* symmetry in the matrix element. Then the form of Eqs. (B2-B5) remains the same when the partial DOS is replaced by the total DOS. Secondly, we neglect the energy dependence, assuming it to be weak in the range of a few eV from the Fermi energy. In Eq. (B4), we neglect the interference term after expanding the modulus square:

$$|M_1^{\sigma\sigma} - M_2^{\sigma\sigma}|^2 = |M_1^{\sigma\sigma}|^2 + |M_2^{\sigma\sigma}|^2 - [M_1^{\sigma\sigma}(M_2^{\sigma\sigma})^* + \text{c.c.}] \approx |M_1^{\sigma\sigma}|^2 + |M_2^{\sigma\sigma}|^2 = 2|M^{\sigma\sigma}|^2. \quad (\text{B6})$$

We have denoted the matrix elements with different energy arguments by $M_1^{\sigma\sigma}$ and $M_2^{\sigma\sigma}$. In the last step, we drop the energy index and use energy-independent matrix elements $M^{\sigma\sigma} = M_1^{\sigma\sigma} = M_2^{\sigma\sigma}$. The approximation of neglecting the interference term was also made by Penn *et al.*¹⁶ The Coulomb matrix elements for scattering between equal and opposite spins are denoted by $M^{\sigma\sigma}$ and $M^{\sigma\bar{\sigma}}$. We use $M^{\uparrow\uparrow} = M^{\downarrow\downarrow}$ and $M^{\uparrow\downarrow} = M^{\downarrow\uparrow}$. For the calculation, we define two parameters for the average matrix element squared and for the ratio of $M^{\uparrow\uparrow}$ and $M^{\uparrow\downarrow}$:

$$M^2 = \frac{|M^{\uparrow\uparrow}|^2 + |M^{\uparrow\downarrow}|^2}{2}, \quad m = \frac{|M^{\uparrow\uparrow}|}{|M^{\uparrow\downarrow}|}.$$

The simplified equations used in the calculations of the scattering rates are given in Eqs. (4-7).

* Corresponding author. Electronic address: roland.knorren@physik.fu-berlin.de

† Present address: Institute for Laser and Plasma Physics, University of Essen, D-45117 Essen, Germany.

¹ C. A. Schmuttenmaer, M. Aeschlimann, H.E. Elsayed-Ali, R.J.D. Miller, D.A. Mantell, J.Cao, and Y. Gao, Phys. Rev. B **50**, 8957 (1994).

² T. Hertel, E. Knoesel, M. Wolf, and G. Ertl, Phys. Rev. Lett. **76**, 535 (1996).

³ J.J. Quinn, Phys. Rev. **126**, 1453 (1962).

⁴ M. Aeschlimann, M. Bauer, and S. Pawlik, Chem. Phys. **205**, 127 (1996).

⁵ S. Ogawa, H. Nagano, and H. Petek, Phys. Rev. B **55**, 10869 (1997).

⁶ E. Knoesel, A. Hotzel, T. Hertel, M. Wolf and G. Ertl, Surf. Sci. **368**, 76 (1996).

⁷ J. Hohlfeld, S.S. Wellershoff, J. Gdde, U. Conrad, V. Jhnke, and E. Matthias, Chem. Phys. **251**, 237 (2000).

⁸ S. Pawlik, M. Bauer and M. Aeschlimann, Surf. Sci. **377-379**, 206 (1997).

⁹ J. Cao, Y. Gao, R.J.D. Miller, H.E. Elsayed-Ali, and D.A. Mantell, Phys. Rev. B **56**, 1099 (1997).

¹⁰ E. Knoesel, A. Hotzel, and M. Wolf, Phys. Rev. B **57**, 12812 (1998).

¹¹ M. Sakaue, H. Kasai, and A. Okiji, J. Phys. Soc. Jpn. **68**, 720 (1999).

¹² H. Petek and S. Ogawa, Prog. Surf. Sci. **56**, 239 (1997).

¹³ H. Petek, H. Nagano, and S. Ogawa, Appl. Phys. B **68**, 369 (1999).

¹⁴ M. Aeschlimann, M. Bauer, S. Pawlik, W. Weber, R. Burgermeister, D. Oberli, and H.C. Siegmann, Phys. Rev. Lett. **79**, 5158 (1997).

¹⁵ M. Aeschlimann, R. Burgermeister, S. Pawlik, M. Bauer, D. Oberli, and W. Weber, J. Elec. Spectros. **88-91**, 179 (1998).

¹⁶ D.R. Penn, S.P. Apell, and S.M. Girvin, Phys. Rev. B **32**, 7753 (1985).

¹⁷ E. Zarate, P. Apell, and P.M. Echenique, Phys. Rev. B **60**, 2326 (1999).

- ¹⁸ E.V. Chulkov, I. Sarria, V.M. Silkin, J.M. Pitarke, and P.M. Echenique, Phys. Rev. Lett. **80**, 4947 (1998).
- ¹⁹ I. Campillo, J.M. Pitarke, A. Rubio, E. Zarate, and P.M. Echenique, Phys. Rev. Lett. **83**, 2230 (1999).
- ²⁰ W.D. Schöne, R. Keyling, M. Bandic, and W. Ekardt, Phys. Rev. B **60**, 8616 (1999).
- ²¹ S. Hüfner, in *Springer Series in Solid State Sciences*, edited by M. Cardona, P. Fulde, K. von Klitzing, H.-J. Queisser, Vol. 82, Ch. 7 (Springer, Berlin, Heidelberg, 1995).
- ²² H.C. Siegmann, Surf. Sci. **307-309** 1076 (1994).
- ²³ S. Ogawa, H. Nagano, H. Petek, and A. P. Heberle, Phys. Rev. Lett. **78**, 1339 (1997).
- ²⁴ C. Timm and K.H. Bennemann, unpublished.
- ²⁵ H. Petek, H. Nagano, and S. Ogawa, Phys. Rev. Lett. **83**, 832 (1999).
- ²⁶ J.M. Ziman, *Principles of the Theory of Solids* (Cambridge University Press, 1972).
- ²⁷ V.L. Moruzzi, J.F. Janak, A.R. Williams, *Calculated Electronic Properties of Metals* (Pergamon, New York, 1978).
- ²⁸ W.A. Harrison, *Electronic Structure and the Properties of Solids* (Freeman, San Francisco, 1979).
- ²⁹ C. Suarez, W.E. Bron, and T. Juhasz, Phys. Rev. Lett. **75**, 4536 (1995).
- ³⁰ R. Knorren, G. Bouzerar, and K. H. Bennemann, unpublished.
- ³¹ J. J. Quinn and R. A. Ferrell, Phys. Rev. **112**, 812 (1958).
- ³² P.M. Echenique, J.M. Pitarke, E.V. Chulkov, and A. Rubio, Chem. Phys. **251**, 1 (2000).
- ³³ D.A. Papaconstantopoulos, *Handbook of the Band Structure of Elemental Solids* (Plenum, New York, 1986).
- ³⁴ Densities of states were calculated by the FLAPW band structure program WIEN95 and were provided by J. Dewitz, private communication (1998).
- ³⁵ H. Eckhardt, L. Fritsche, and J. Noffke, J. Phys. F, Met. Phys. **14**, 97 (1984).
- ³⁶ P.B. Johnson and R.W. Christy, Phys. Rev. B **6**, 4370 (1972); Phys. Rev. B **9**, 5056 (1974).
- ³⁷ R. Knorren and K.H. Bennemann, Appl. Phys. B **68**, 401 (1999).
- ³⁸ E. Knoesel, Ph.D. thesis, Freie Universität Berlin (1997).
- ³⁹ H.C. Siegmann, J. Phys., Condens. Matter **4** 8395 (1992).
- ⁴⁰ J. Kirschner, in *Polarized Electrons in Surface Physics*, edited by R. Feder (World Scientific, Singapore, 1985).
- ⁴¹ W. Weber, A. Bischof, and R. Allenspach, Phys. Rev. B **54**, 4075 (1996).
- ⁴² P. Krams, F. Lauks, R.L. Stamps, B. Hillebrands, and G. Günterodt, Phys. Rev. Lett. **69**, 3674 (1992).
- ⁴³ J. Thomassen, F. May, B. Feldmann, M. Wuttig, and H. Ibach, Phys. Rev. Lett. **69**, 3831 (1992).
- ⁴⁴ F. Scheurer, R. Allenspach, P. Xhonneux, and E. Courtens, Phys. Rev. B **48**, 9890 (1993).
- ⁴⁵ R. Naik, M Ahmad, G.L. Dunifer, C. Kota, A. Poli, Ke Fang, U. Rao, and J.S. Payson, J. Magn. Magn. Mat. **121**, 60 (1993).
- ⁴⁶ G. Bochi, C.A. Balentine, H.E. Inglefield, S.S. Bogomolov, C.V. Thompson, and R.C. O'Handley, J. Appl. Phys. **75**, 6430 (1994).
- ⁴⁷ M. Bauer, S. Pawlik, and M. Aeschlimann, Phys. Rev. B **55**, 10040 (1997).
- ⁴⁸ M. Bauer, S. Pawlik, and M. Aeschlimann, Phys. Rev. B **60**, 5016 (1999).
- ⁴⁹ M. Bauer, S. Pawlik, R. Burgermeister, and M. Aeschlimann, Surf. Sci., **402-404**, 62 (1998).
- ⁵⁰ J. Friedel, in *Physics of Metals*, edited by J. M. Ziman, Vol. 1, Ch. 8 (Cambridge University Press, Cambridge, 1969).
- ⁵¹ J.B. Mann, *Atomic Structure Calculations*, Los Alamos Sci. Lab. Rept. LA-3690 (1967).
- ⁵² R. Matzdorf, A. Gerlach, F. Theilmann, G. Meister, and A. Goldmann, Appl. Phys. B **68**, 393 (1999).

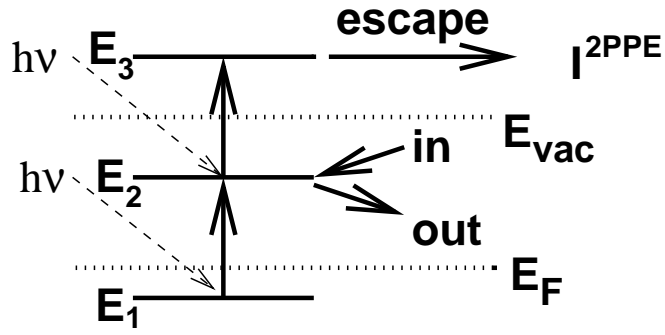


FIG. 1. Illustration of the monochromatic 2PPE process with initial state E_1 , intermediate state E_2 and final state E_3 . A first photon excites an electron from an initial level E_1 in the range between E_F and $E_F - h\nu$ into a level E_2 . The population $f(E_2, t)$ depends on the temporal pulse shape of the exciting laser and is time-dependent due to electron-electron interaction and transport of electrons out of the optically excited region into the bulk. A second photon excites an electron with energy E_2 into a state E_3 above the vacuum energy E_{vac} , from which it can contribute to the 2PPE intensity via $I^{2\text{PPE}}(E_3, t) \propto f(E_2, t)$.

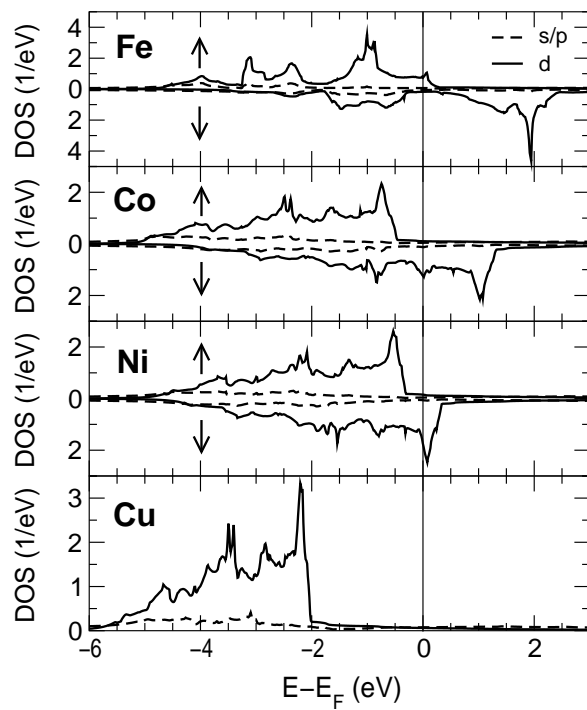


FIG. 2. LAPW density of states (DOS) used as input in the calculation of the electron-electron scattering rates in Eqs. (4–7).

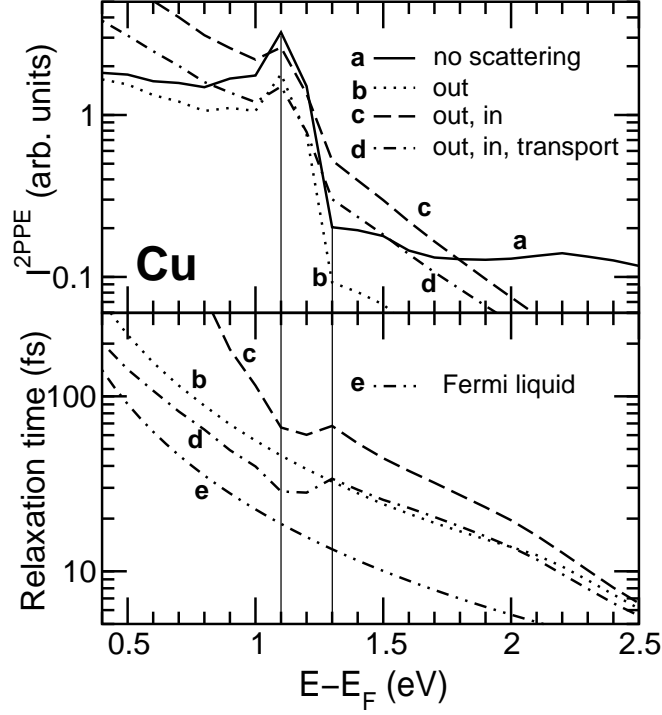


FIG. 3. Calculated 2PPE intensity and relaxation time of the excited electron distribution for Cu for photon energy $h\nu = 3.3$ eV. Curve *a* shows the 2PPE intensity if no scattering is present and reflects the distribution of optically excited electrons. Curve *b* gives the result if only scattering out of the intermediate level is kept in Eq. (2). Curve *c* is the result if scattering into the intermediate state (secondary electron effect) is also included. Curve *d* represents the case when the effect of transport is also taken into account. The relaxation time when only scattering out of the intermediate state is kept (curve *b*) is a single-electron lifetime and can be compared with the lifetime predicted by Fermi-liquid theory, shown in curve *e*. The other relaxation times are effective relaxation times of the distribution of excited electrons.

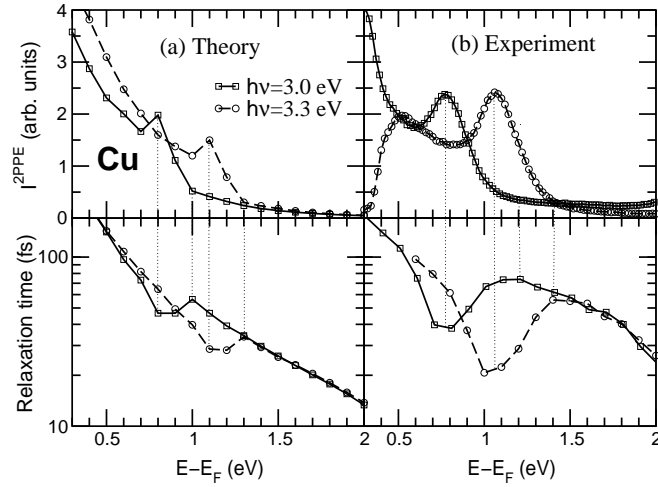


FIG. 4. Calculated (a) and measured (b) 2PPE intensity and relaxation time for Cu for photon energies $h\nu = 3.0$ and 3.3 eV. Calculations include secondary electrons and transport. Note the dependence of the relaxation time on photon energy, especially in the region of the peak in the intensity ($E - E_F = 0.7 - 1.3$ eV). The minimum in the relaxation time corresponds to the peak in the intensity and the maximum in the relaxation time corresponds to the d -band threshold, as indicated by the dotted lines, in agreement with several experiments.⁸⁻¹⁰

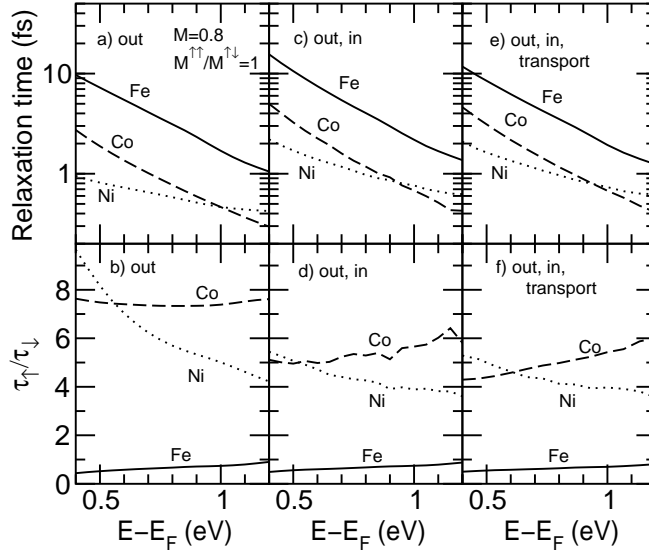


FIG. 5. Spin-averaged relaxation time of the distribution and ratio of relaxation times for majority and minority electrons. Results labelled *out* are single-electron lifetimes. Results (*out, in*) refer to relaxation times of the distribution including secondary electrons. Results (*out, in, transport*) also include transport. The same average Coulomb matrix element $M = 0.8$ eV and $|M^{\uparrow\uparrow}/M^{\uparrow\downarrow}| = 1$ is used.

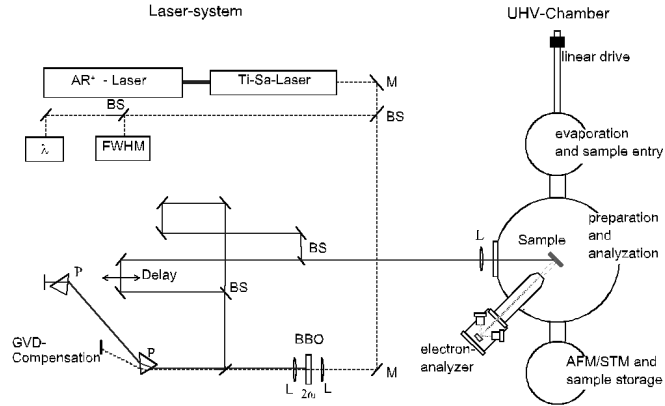


FIG. 6. Schematic view of the equal pulse correlation set-up for time resolved 2PPE.

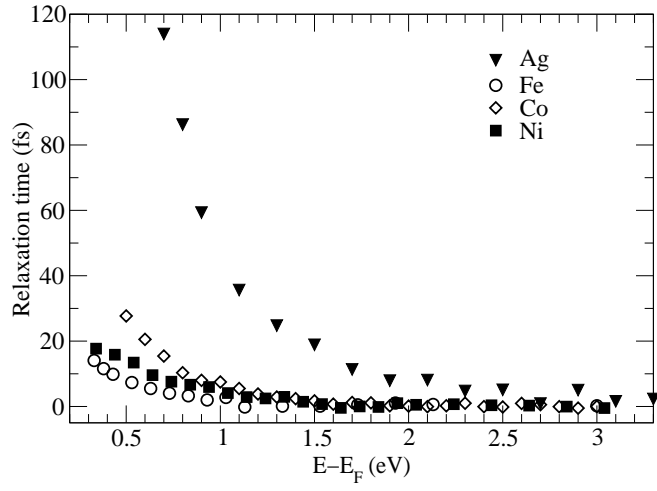


FIG. 7. Comparison of experimental relaxation time results for Ag and the three transition metals, Fe, Co, and Ni.

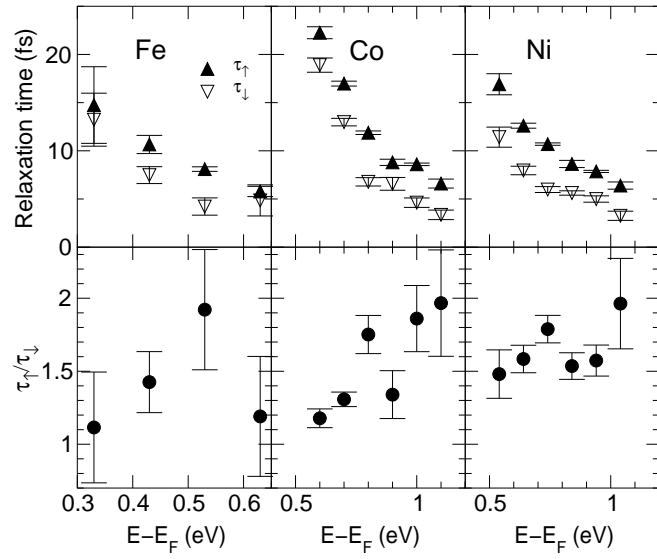


FIG. 8. Experimental results for the spin-resolved relaxation time τ_{\uparrow} and τ_{\downarrow} and the ratio $\tau_{\uparrow}/\tau_{\downarrow}$ of majority to minority relaxation time.

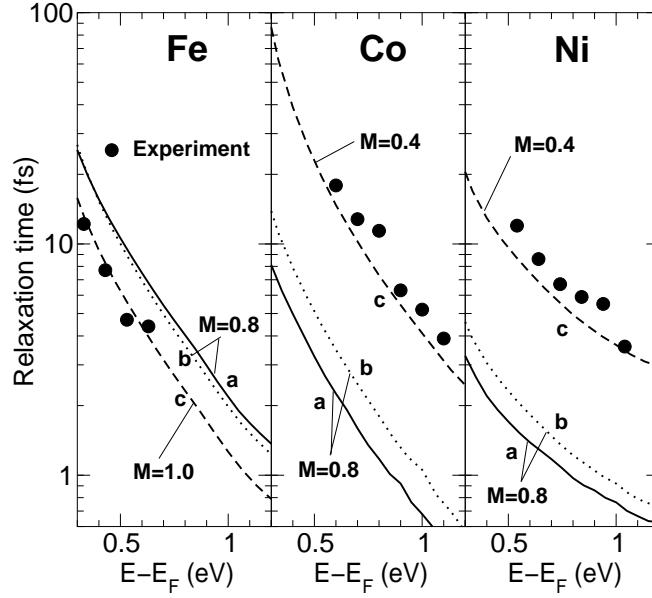


FIG. 9. Experimental and theoretical results for the spin-averaged relaxation time of the distribution. Calculations include secondary electron effects. Curve *a* shows results using Coulomb matrix element $M = 0.8$ eV and $|M^{\uparrow\uparrow}/M^{\uparrow\downarrow}| = 1$ for the various transition metals. Curve *b* gives results for the same M , but $|M^{\uparrow\uparrow}/M^{\uparrow\downarrow}| = 0.5$. Results using different values of M for the various transition metals and $|M^{\uparrow\uparrow}/M^{\uparrow\downarrow}| = 0.5$ are shown in curve *c*.

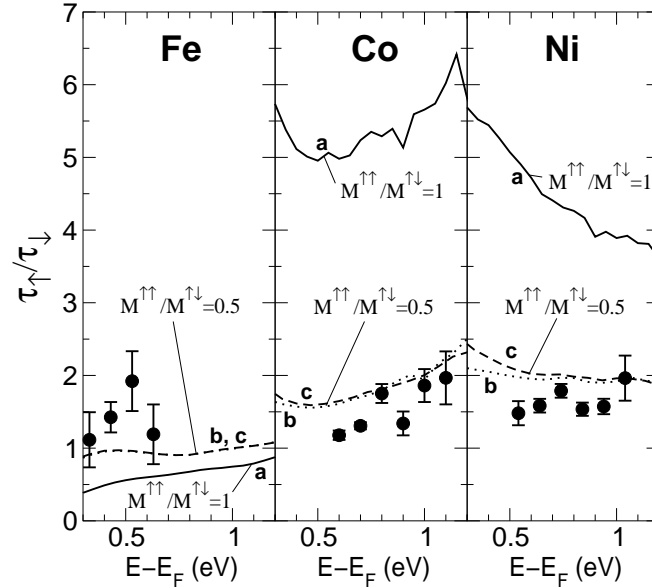


FIG. 10. Experimental and theoretical results for the ratio $\tau_{\uparrow}/\tau_{\downarrow}$ of the relaxation time of the distribution. The labels are as in Fig. 9 and refer to the same parameters.

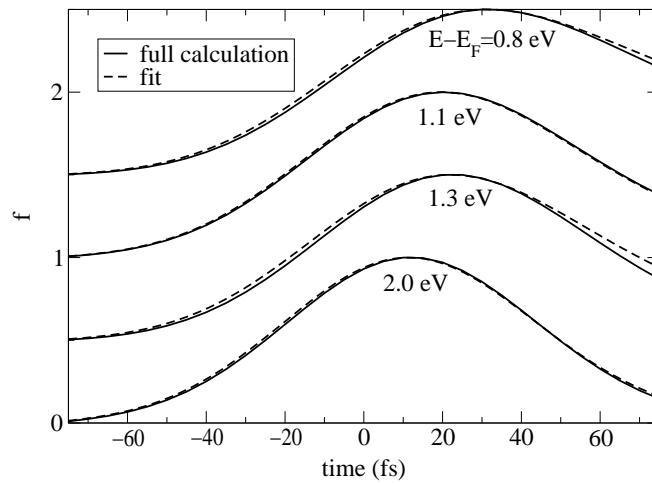


FIG. 11. Calculated occupation function for different intermediate state energies (normalized to 1 at the maximum) and fit by a function describing exponential decay. The calculation is for Cu with $h\nu = 3.3$ eV and a pump laser of 70 fs duration.